Atmos. Chem. Phys. Discuss., 7, 14895–14937, 2007
www.atmos-chem-phys-discuss.net/7/14895/2007/

Atmospheric
Chemistry
and Physics
Discussions

GEM-AQ, an on-line global multiscale chemical weather system: model description and evaluation of gas phase chemistry processes

J. W. Kaminski[1], **L. Neary**[1], **J. Struzewska**[2], **J. C. McConnell**[1], **A. Lupu**[1], **J. Jarosz**[1], **K. Toyota**[1], **S. L. Gong**[3], **J. Côté**[4], **X. Liu**[5,*], **K. Chance**[5], **and A. Richter**[6]

[1] Centre for Research in Earth and Space Science, Atmospheric Modelling and Data Assimilation Laboratory, York University, Toronto, Canada
[2] Institute of Environmental Engineering Systems, Warsaw University of Technology, Warsaw, Poland
[3] Science and Technology Branch, Environment Canada, Toronto, Canada
[4] Science and Technology Branch, Environment Canada, Montréal, Canada
[5] Smithsonian Astrophysical Observatory, Cambridge, MA, USA
[6] Institute of Environmental Physics, University of Bremen, Germany
[*] now at: Goddard Earth Sciences and Technology, University of Maryland Baltimore County, Baltimore, MD, USA

Received: 23 August 2007 – Accepted: 4 October 2007 – Published: 16 October 2007

Correspondence to: J. W. Kaminski (jacek@yorku.ca)

Abstract

Tropospheric chemistry and air quality processes were implemented on-line in the Global Environmental Multiscale model. The integrated model, GEM-AQ, has been developed as a platform to investigate chemical weather at scales from global to urban. The model was exercised for five years (2001–2005) to evaluate its ability to simulate seasonal variations and regional distributions of trace gases such as ozone, nitrogen dioxide and carbon monoxide on the global scale. The model results presented are compared with observations from satellites, aircraft measurement campaigns and balloon sondes.

1 Introduction

The strategic objective of our project was to develop and evaluate a modelling system for tropospheric chemistry and air quality. In our design we have selected the Global Environmental Multiscale model (GEM) (Côté et al., 1998a) as a host meteorological model for inclusion of air quality processes. The GEM model was developed at the Canadian Meteorological Centre and is used for operational weather prediction in Canada. The GEM model was augmented by implementing air quality chemistry, including the gas phase, aerosol and cloud particles, limited wet chemistry, emission, deposition and transport processes.

The integrated model, which we here call GEM-AQ, serves as a platform for performing scientific studies on processes and applications. The GEM-AQ model has been run for a number of scenarios ranging from a global uniform domain (this study), global variable resolution for regional scenarios (O'Neill et al., 2006), to high resolution studies, i.e. Struzewska and Kaminski (2007). GEM-AQ has also been augmented to study persistent organic pollutants (POPs) globally (Gong et al., 2007; Huang et al., 2007).

GEM-AQ has been exercised with a 5 year simulation (2001–2005) on a global uniform 1.5°×1.5° resolution domain (240×120 grid points) and 28 hybrid levels extending to 10 hPa. The objectives of this simulation were to derive a multi-year model climatology, to examine seasonal variation and regional distribution, evaluate global emissions, and provide chemical initial and boundary conditions for high resolution model simulations.

In order to evaluate the model, we compare simulated ozone with ozonesonde observations from SHADOZ (Southern Hemisphere ADditional OZonesondes) (Thompson et al., 2003a,b) as well as climatological ozonesonde observations (Logan, 1999), GOME (Global Ozone Monitoring Experiment) satellite observations (Burrows et al., 1999) and surface station data (World Data Centre for Greenhouse Gases, http://gaw.kishou.go.jp/wdcgg.html). Modelled nitrogen dioxide is compared with SCIAMACHY (Scanning Imaging Absorption Spectrometer for Atmospheric Cartography) (Burrows et al., 1995; Bovensmann et al., 1999) and aircraft campaigns such as TRACE-A (Transport and Atmospheric Chemistry near the Equator-Atlantic) (Fishman et al., 1996) are used to evaluate other species such as nitric acid, hydrogen peroxide and others. Modelled CO concentrations are compared with MOPITT (Measurements Of Pollution In The Troposphere) (Drummond, 1992; Drummond and Mand, 1996) satellite data.

2 Modelling approach

In order to develop an air quality modelling system which can accommodate various scales and processes, we have used the GEM model as a computational platform and environmental processes were implemented on-line. There is a growing recognition for on-line implementation of tightly coupled environmental processes. Similar implementation of environmental processes is done in WRF/Chem (Weather Research and Forecasting model with Chemistry) (Grell et al., 2005), MC2-AQ (Mesoscale Compressible Community model with Air Quality) (Kaminski et al., 2002), MESSy (Modular Earth Submodel System) (Jöckel et al., 2006), RAMS (Regional Atmospheric Modeling

System) (Marécal et al., 2006) and Méso-nh (non-hydrostatic mesoscale atmospheric model) (Tulet et al., 2003).

The on-line implementation of environmental processes in the GEM model allows us to run in global uniform, global variable, and limited area configurations, allowing for multiscale chemical weather modelling. This approach provides access to all required dynamics and physics fields for chemistry at every time step. The on-line implementation of chemistry and aerosol processes will allow for introducing feedback on model dynamics and physics. The use of the GEM framework permits the incorporation of chemical data assimilation techniques into the model validation and application studies in a unified fashion.

The developed modelling system can be used to plan field campaigns, interpret measurements, and provide the capacity for forecasting oxidants, particulate matter and toxics. Also, it can be used to provide guidance to evaluate exposure studies for people, animals, crops and forests, and possibly for epidemiological studies.

2.1 Host meteorological model

The host meteorological model used for air quality studies is the Global Environmental Multiscale (GEM) model. GEM can be configured to simulate atmospheric processes over a broad range of scales, from the global scale down to the meso-γ scale.

2.1.1 Model dynamics

The set of non-hydrostatic Euler equations (with a switch to revert to the hydrostatic primitive equations) maintain the model's dynamical validity right down to the meso-γ scales. The time discretization of the model dynamics is fully implicit, 2 time-level (Côté et al., 1998a,b). The spatial discretization for the adjustment step employs a staggered Arakawa C grid that is spatially offset by half a mesh length in the meridional direction with respect to that employed in previous model formulations. It is accurate to second order, whereas the interpolations for the semi-Lagrangian advection are of fourth-order accuracy, except for the trajectory estimation (Yeh et al., 2002). The vertical diffusion of momentum, heat and tracers is a fully implicit scheme based on turbulent kinetic energy (Benoît et al., 1989). GEM version 3.1.2 was used in the current study.

2.1.2 Model physics

The physics package consists of a comprehensive set of physical parameterization schemes (Benoît et al., 1989; Mailhot et al., 1989; Mailhot, 1994). Specifically, the planetary boundary layer is based on a prognostic equation for turbulent kinetic energy (Benoît et al., 1989). Shallow convection is simulated using a method described by Mailhot (1994) and is treated as a special case of the turbulent planetary boundary layer to include the saturated case in the absence of precipitation. Over land, in this version, the surface temperature is calculated using the force-restore method (Deardorff, 1978; Benoît et al., 1989) combined with a stratified surface layer. Deep convective processes are handled by a Kuo-type convective parameterization (Kuo, 1974; Mailhot et al., 1989) for the resolutions that we have adopted for this study. The infrared radiation scheme (Garand, 1983; Garand and Mailhot, 1990; Yu et al., 1997) includes the effects of water vapour, carbon dioxide, ozone, and clouds. The solar radiation scheme follows the method described by Fouquart and Bonnel (1980). Gravity wave drag parameterization is based on a simplified linear theory for vertically propagating gravity waves generated in statically stable flow over mesoscale orographic variations (McFarlane, 1987; McLandress and McFarlane, 1993). GEM physics package version 4.2 was used in the current study.

2.2 Air quality modules

Air quality modules are implemented on-line in the host meteorological model. Currently, there are 37 advected and 14 non-advected gas phase species in the model, shown in Table A1. Transport of the chemically active tracers by the resolved circulation is calculated using the semi-Lagrangian advection scheme native to GEM. The vertical transfer of trace species due to subgrid-scale turbulence is parameterized using eddy diffusion calculated by the host meteorological model. Large scale deep convection in the host model depends on the resolution: in this version of GEM-AQ we use the mass flux scheme of Zhang and McFarlane (1995) for tracer species.

2.2.1 Gas phase chemistry

The gas-phase chemistry mechanism currently used in the GEM-AQ model is based on a modification of version two of the Acid Deposition and Oxidants Model (ADOM) (Venkatram et al., 1988), derived from the condensed mechanism of Lurmann et al. (1986). The ADOM-II mechanism comprises 47 species, 98 chemical reactions and 16 photolysis reactions. In order to account for background tropospheric chemistry, 4 species (CH_3OOH, CH_3OH, CH_3O_2 and CH_3CO_3H) and 22 reactions were added. All species are solved using a mass-conserving implicit time stepping discretization, with the solution obtained using Newton's method. Heterogeneous hydrolysis of N_2O_5 is calculated using the on-line distribution of aerosol. The list of chemical and photolysis reactions is given in Table A2 and Table A3, respectively.

Although the model meteorology is calculated to 10 hPa, the focus of the chemistry is in the troposphere where all species are transported throughout the domain. To avoid the overhead of stratospheric chemistry in this version (a combined stratospheric/tropospheric chemical scheme is currently being developed) we replaced both the ozone and NO_y fields with climatologies above 100 hPa after each transport time step. This ensures a reasonable upper boundary to the troposphere, while ensuring that the transport of ozone and NO_y fields to the troposphere is well characterised by the model dynamics. For ozone we used the HALOE (Halogen Occultation Experiment) climatology (e.g. Hervig et al., 1993), while NO_y fields are taken from the CMAM (Canadian Middle Atmosphere Model) (e.g. de Grandpré et al., 2000). Photolysis rates (J values) are calculated on-line every chemical time step using the method developed by Landgraf and Crutzen (1998). In this method, radiative transfer calculations are done using a delta-two stream approximation for 8 spectral intervals in the UV and visible applying precalculated effective absorption cross sections. This method also allows for scattering by cloud droplets and for clouds to be present over a fraction of a grid cell. Both cloud cover and water content are provided by the host meteorological model. The J value package used was developed for MESSy (Jöckel et al., 2006) and has been implemented in GEM-AQ.

2.2.2 Aerosol package

The current version of GEM-AQ has 5 size-resolved aerosols types, viz. sea salt, sulphate, black carbon, organic carbon, and dust. The microphysical processes which describe formation and transformation of aerosols are calculated by a sectional aerosol module (Gong et al., 2003). The particle mass is distributed into 12 logarithmically spaced bins from 0.005 to 10.24 microns radius. This size distribution leads to an additional 60 advected tracers. The following aerosol processes are accounted for in the aerosol module: nucleation, condensation, coagulation, sedimentation and dry deposition, in-cloud oxidation of SO_2, in-cloud scavenging, and below-cloud scavenging by rain and snow.

2.2.3 Gas-phase removal processes

The effects of dry deposition are included as a flux boundary condition in the vertical diffusion equation. Dry deposition velocities are calculated from a ‘big leaf’ multiple resistance model (Wesely, 1989; Zhang et al., 2002) with aerodynamic, quasi-laminar layer, and surface resistances acting in series. The process assumes 15 land-use types and takes snow cover into account.

GEM-AQ only has a simplified aqueous phase reaction module for oxidation of SO_2 to sulphate. Thus, for the gas phase species, wet deposition processes are treated in a simplified way. Only below-cloud scavenging of gas phase species is considered in the model. The efficiency of the rainout is assumed to be proportional to the precipitation rate and a species-specific scavenging coefficient. The coefficients applied are the same as those used in the MATCH model (Multiscale Atmospheric Transport and Chemistry Model) used by the Swedish Meteorological and Hydrological Institute (SMHI) (Langner et al., 1998).

2.2.4 Emissions

The emission dataset used for global simulations was compiled using EDGAR 2.0 (Emission Database for Global Atmospheric Research) (archived in 2000, valid for 1990) and GEIA (Global Emissions Inventory Activity) global inventories (Olivier et al., 1999; Olivier and Berdowski, 2001). The EDGAR 2.0 data was chosen for its detailed information on non-methane volatile organic compound speciation. Emission data compiled for GEM-AQ includes global fields of anthropogenic emission fluxes with $1^\circ \times 1^\circ$ resolution and natural emissions with $5^\circ \times 5^\circ$ resolution. Yearly averaged anthropogenic emissions contain different industrial sectors and non-industrial activity such as burning of agricultural wastes and fuel wood, for 14 gaseous pollutants. Monthly averaged biogenic, ocean and soil emission fluxes, as well as biomass burning (forest and savannah) emissions, have been derived for 9 species (7 VOC species, CO and NO_2). The various species for which emissions are included, along with source type, viz. anthropogenic combustion, biomass burning, are given in Table A4. In the upper troposphere/lower stratosphere region (UTLS) sources of NO_x are small, from large scale convective updrafts, stratospheric sources, aircraft and lightning. We have used the monthly mean totals of lightning NO_x from the GEIA inventory (scaled from 12.2 Tg/yr to 2 Tg/yr) and distributed them in the horizontal according to the convective cloud distribution of the model. In the vertical, the lightning NO_x is distributed according to the profiles given by Pickering et al. (1993). No aircraft emissions were used in the present simulations.

3 Model simulation and results

For the simulations carried out in the current study the model was configured with 28 vertical levels with model top at 10 hPa. To better account for stratospheric/tropospheric exchange in polar regions and, in particular, ozone inflow from the stratosphere, a hybrid vertical coordinate system (Laprise and Girard, 1990) was used. A sponge layer is present to prevent reflected waves at the top of the model and acts on the top model level.

The horizontal model grid was set as non-rotated uniform-resolution latitude-longitude mesh with the resolution of 1.5°, resulting in 240 by 120 grid points on a sphere. The model time step was set to 1800 seconds for dynamics, physics and air quality processes. Meteorological initial conditions were taken from the Canadian Meteorological Centre global assimilation system (Gauthier et al., 1999, 2007; Laroche et al., 2007). The GEM-AQ model was run in 24 h forecast segments starting from 6-h trial fields generated in a separate GEM execution. This setup resulted in meteorological fields being forced to observations once a day.

The chemical initial conditions used to initiate the model for the first time were generated from several sources. Chemical fields in the upper troposphere and lower stratosphere were taken from the CMAM model (de Grandpré et al., 2000) for January. In order to create a balanced and realistic chemical state, GEM-AQ was spun up for 6 months. This initial period was not used in the analysis of model results. In addition, a number of fields and parameters are needed to specify surface characteristics. These are obtained from analysed climatological and geophysical datasets and include surface roughness, land-sea mask, albedo, deep soil temperature, ice cover, and topography. The surface roughness length is influenced by topography, land use, snow and ice cover.

3.1 Ozone

One of the basic species which drives tropospheric chemistry is ozone and so it is essential for a model to provide a reasonable spatial and temporal representation of the 3-D ozone field. Thus we have compared seasonally averaged GEM-AQ model ozone profiles from 2001–2005 with ozonesonde data compiled by Logan (1999) for the 1980s and 1990s.

The comparison of ozonesondes with model results consistently shows good agreement with the observations, although the region between 300 and 100 hPa tends to be under-predicted in most areas of the globe for all seasons. This height range is where the ozonesonde measurements show the most variability. Interestingly, we have found that use of sigma coordinates caused an excess of ozone influx in regions of high topography such as over the Himalayas and Greenland. This resulted in too much upper tropospheric ozone in the northern hemisphere. Changing to the hybrid coordinate reduced the flux. Figure 1 shows seasonally averaged vertical profiles for two stations, Churchill (59° N, 94° W)and Hohenpeissenberg (48° N, 11° E).

In general, the agreement with all the stations is quite similar. Some ozonesonde stations show a summer model over-prediction in the lowest levels. This may be due to the dilution of emissions over relatively larger grid squares where ozone production is more efficient at lower mixing ratios (Liu et al., 1987).

To examine the model performance in the tropics where deep convection and lightning play a role in the distribution of ozone, the SHADOZ dataset (Thompson et al., 2003a,b) was used. Figure 2 shows a comparison of seasonally averaged SHADOZ ozonesondes and temperature measurements at four stations in the South Pacific with GEM-AQ results for 2001. There is an over-prediction in this region, likely due to an incorrect diagnosis of deep convective cloud and therefore the generation of ozone from lightning generated NO_x is not captured correctly. The individual ozonesonde profiles (not shown here) indicate that this may be the case.

Comparison with ozonesondes gives detailed vertical resolution but over a limited spatial region. Another method to evaluate the model is to compare ozone data with more limited vertical resolution but much more comprehensive horizontal spatial coverage. For this aspect of the study we have compared model results with tropospheric ozone columns from GOME, a nadir viewing instrument on ESA's ERS-2 satellite. GOME tropospheric data have been validated against contemporaneous ozonesonde data (Liu et al., 2005, 2006).

Both GOME and GEM-AQ tropospheric columns are calculated using a tropopause determined by combining the dynamic tropopause in the extratropics and the thermal tropopause near the equator (Liu et al., 2006). In order to account for the different spatial resolutions of the GOME retrievals and GEM-AQ runs, model output profiles corresponding to the model grid cells overlapping each GOME pixel were interpolated onto the GOME vertical levels, then averaged using the relative surface area of the corresponding GOME pixel and the GEM-AQ cell intersection as a weight. The GOME averaging kernel was then applied to the averaged model profile, and the tropospheric column calculated by integrating the transformed profile up to the tropopause level. Finally, all the column data (GOME and model) were mapped onto the model grid by the same area-weighting method, and the monthly means obtained.

Figure 3 shows the GEM-AQ, GOME and GOME-GEM differences in tropospheric ozone column for April, July and October, 2001. In April, GEM-AQ under-predicts in the high northern latitudes (>30° N) with differences of 5–10 DU. This agrees with the comparison with the ozonesondes. In the tropical ocean regions, GEM-AQ has ozone columns as large as 15 DU too large compared with GOME. This is consistent with the results compared with SHADOZ. For southern latitudes GEM-AQ has differences less than 10 DU. For July the pattern is much the same, although a plume off the coast of China is not captured by the model. For October, GEM-AQ over-predicts by 5–10 DU over most of the globe. Only over the southern Pacific does the disagreement reach 15 DU. This might be because GEM-AQ is not capturing the timing and distribution of NO_x generation by lightning, as mentioned above. The method that we have adopted relies on the modelled deep convective cloud, which may put too much NO_x over the ocean.

Many of the important processes involved in the study of air quality take place near the surface. Surface data gathered from the World Data Centre for Greenhouse Gases (http://gaw.kishou.go.jp/wdcgg.html) provides an opportunity to analyse the model performance in detail. Figure 4 shows surface ozone data from two stations , Yonagunijima (24° N, 123° E) and Algoma (47° N, 84°W) for 2001. The agreement for the Japanese station is quite good. Generally the model captures the background levels. Many of the excursions from the background are captured, such as in late February, April and the general elevation of the background in September. However, there are some occurrences of plumes not shown in the measurements, and some elevated values are modelled too high. For the Canadian station chosen the agreement between measurements and model is quite acceptable. The incidents in June and July and much of the variability of the measurements are captured.

3.2 Carbon monoxide

Carbon monoxide has a chemical lifetime of a few months or longer in the troposphere, depending on latitude and season. It can be a very useful tracer of the resolved transport, but also impacted, of course, by large scale convection and transport in the planetary boundary layer. Thus, a comparison with observations serves as a useful diagnostic of both transport and emissions in the model. In the following section we compare model results with the CO data from the MOPITT instrument (Drummond, 1992; Drummond and Mand, 1996) on the NASA Terra satellite. MOPITT is a nadir viewing instrument and, like GOME, has limited vertical resolution and is most sensitive at about 500 hPa. For this study we compare with the CO volume mixing ratio data obtained from the MOPITT instrument for 500 and 850 hPa. The MOPITT kernel has been applied to the GEM-AQ data.

Figure 5 shows the 500 hPa data for January and October, 2002 for GEM-AQ and MOPITT. For most times of the year, GEM-AQ captures the general pattern of the measured CO quite well. In January there is good agreement between GEM-AQ and

MOPITT data at 500 hPa, although GEM-AQ, as revealed by the mixing ratios, appears to have too high biomass burning emissions over Amazonia.

In October, Northern hemisphere CO values at 500 hPa are in general agreement with MOPITT data except over China, where GEM-AQ over-predicts CO. In the southern hemisphere the signal from biomass burning over southern Africa is too small compared to MOPITT data, although the agreement over Amazonia is reasonable. However, GEM-AQ completely misses the heavy biomass burning that occurred over Indonesia (Edwards et al., 2006) since it uses climatological emissions. Perhaps as a result of the biomass burning emissions, GEM-AQ does not produce as high values in the southern subtropics: the plumes from Africa and South America only extend to Australia and Africa, respectively.

Figure 6 shows the MOPITT CO mixing ratios for the 850 hPa level for the same months as Fig. 5. The strengths and weaknesses of the model predictions at this level are similar to the 500 hPa comparison. For January, GEM-AQ does quite a reasonable job in both hemispheres, although biomass emissions in southwest Africa seem displaced southward in GEM-AQ for this year. Also, GEM-AQ CO levels appear on the high side over Amazonia but appear too low over Australia.

For October, the 850 hPa GEM-AQ CO mixing ratios are too low by about 20%. In particular, CO values are low over the northeast coast of China and Indonesia and most of the southern subtropics except for Amazonia.

One interesting feature that is not reproduced in the model results are high values of CO over the Sahara Desert at the 850 hPa level: there is either no suitable source or the winds do not appear to transport CO across the tropics. This is a recurrent feature of the 850 hPa MOPITT data and it might represent an artefact of the retrieval process.

3.3 Nitrogen dioxide

Nitrogen dioxide is an important species for the generation of ozone in the troposphere. It has a relatively short lifetime (less than a week) so it is closely linked to emission sources. NO and NO_2 are closely related and the daytime ratio of NO to NO_2 rapidly increases with height in the troposphere so that most of the NO_2 is concentrated in the first few kilometres. These characteristics allow the retrieval of NO_x emissions from space (Martin et al., 2006). The SCIAMACHY instrument (Burrows et al., 1995; Bovensmann et al., 1999) on ESA's EVISAT performs measurements in the UV-vis and near IR using solar occultation, limb viewing of scattered light and also observation of scattered light in the nadir direction. In the latter mode it is similar to GOME but has a higher horizontal spatial resolution (typically 60 km×30 km). In this section we compare the NO_2 tropospheric column measurements from SCIAMACHY with the GEM-AQ column NO_2. As SCIAMACHY measures the total vertical column of NO_2 the stratospheric component must be subtracted. This is also done for the GEM-AQ results as the simulation extends into the stratosphere. Using the Canadian Middle Atmosphere Model (CMAM) (de Grandpré et al., 2000) we note that the daytime longitudinal variability of NO_2 is quite large and varies by ±20% and this likely limits the accuracy of lower NO_2 columns. Also, as for GOME and MOPITT, cloud contamination can also cause problems. In Fig. 7 we present GEM-AQ and SCIAMACHY column data for September 2004 and January 2005 using a logarithmic scale because of the large variability of tropospheric NO_2. The SCIAMACHY tropospheric column was computed by subtracting the total column over a clean reference sector in the Pacific, between 180°and 220°. This column is assumed to be the stratospheric contribution only. For comparison with GEM-AQ, the SCIAMACHY data is shown on the same $1.5^\circ \times 1.5^\circ$ grid. For the GEM-AQ results, the same clean reference sector method was used. The tropospheric column was also computed using the thermal tropopause and was found to be about 25% higher than the clean sector method in relatively unpolluted regions and through the tropics. This may suggest the reference sector in GEM-AQ has an excess of tropospheric NO_2, perhaps from lightning emissions.

In Fig. 7, for September, the agreement is good in regions where anthropogenic emissions dominate, such as North America and Europe. However, column NO_2 over China is under-estimated by an order of magnitude. This same pattern is shown in January. In Africa and South America, the values are generally under-estimated. In this region, using the thermal tropopause to determine the column gives better agreement. Again, this is probably due to an excess of lightning NO_x in the reference sector. In January, a low density plume can be seen from North America over the Atlantic by both the model and observations.

Figure 8 presents correlation diagrams between SCIAMACHY and GEM-AQ for September and January for the globe, North and South America, Europe, Africa and China. The regional boundaries are shown in Fig. 9 and are over the continental surfaces only, not including the surrounding oceans.

For September and January the global picture is that SCIAMACHY NO_2 columns are relatively high compared to GEM-AQ. At the low end of mixing ratios there is more variability as might be expected. A perusal of the individual regions reveals the source of the bias. For China, South America and Africa both January and September exhibit strong biases for NO_2 columns above about $1{-}2\times10^{15}$ molecules/cm^2 but for smaller columns there is relatively good agreement. For North America there is quite good agreement. The bias over Africa is reduced when the NO_2 tropospheric column is computed using the thermal tropopause rather than the clean sector method. This is not the case over China, indicating the anthropogenic emissions used in the simulation may be too low.

3.4 Other species

Global coverage of species other than O_3, NO_2 and CO is not as readily available. However, aircraft campaigns can provide a local but comprehensive chemical picture of the troposphere. While the aircraft campaigns are for a specific weather situation not covered by our simulation, they are still useful. We have addressed the specific weather situation covering boreal forest burning in Quebec (O'Neill et al., 2005) and air quality in recent European heat waves (Struzewska and Kaminski, 2007). Nevertheless, to assess some of the other species in the model we have made a comparison with the chemical measurements of the TRACE-A campaign during 1992 (Fishman et al., 1996). Clearly, since the years are quite different, we do not expect the same degree of agreement as one would aim for in a comparison for that specific time period. However, we do compare observations taken during TRACE-A from 21 September to 26 October 1992 with model results for the same period August 2001 so that the same general weather features might be present. The results averaged over the whole period for CH_3CHO, C_2H_6, C_3H_8, CH_2O, PAN, O_3, NO, HNO_3, H_2O_2, DIAL O_3, CO and CH_3OOH are shown in Fig. 10a to l, respectively. The focus of the TRACE-A campaign was to study the cause and source of high concentrations of ozone over the tropical Atlantic Ocean between southern Africa and South America. This season is a period of intense burning of vegetation, resulting in high concentrations of ozone in this region. Overall, the averaged results during the period compare well for all species, including CO and hydrocarbons, considering that climatological emissions were used. The variability of the measurements is not seen in the model because of this, and values are slightly under-predicted. Too much methyl peroxide (CH_3OOH) in the lowest layers and relatively good agreement of H_2O_2 might indicate that the convective transport modelled is insufficient during this period, as CH_3OOH is less soluble than H_2O_2 and is able to be transported into the upper troposphere. The observed NO profile shown in Fig. 10g has the "c" shape that is associated with NO_x from convection, where the model profile is not as clearly defined.

4 Discussion and conclusions

In this study we have focused on the large scale properties of the presented modelling system. This limited comparison indicates that GEM-AQ is, in general, able to capture the spatial details of the chemical fields in the middle and lower troposphere. The comparison with GOME and SHADOZ shows the largest discrepancy over the tropical oceans. Some of the problem may be due to our treatment of deep convection and resulting lightning NO_x emissions. A more detailed study of the modelled convective activity is under way. Other limitations may be due to the use of seasonally averaged biomass burning emissions. We have developed an emission system for boreal and tropical fires based on monthly biomass burning emissions at 1°×1° spatial resolution for year 2004 from the Global Fire Emission Database version 2 (GFEDv2) but distributed into hourly emissions using fire counts from the Geostationary Operational Environmental Satellite (GOES) Wild Fire Automated Biomass Burning Algorithm (WF_ABBA) fire product as weighting factors (Lupu et al., 2007[1]). This work also showed sensitivity to the height distribution of emissions. For the simulations presented here, the biomass burning emissions were injected into the lowest layer only. Another reason for the large ozone values in the tropics and low values in the northern hemisphere may be due to a weak Brewer-Dobson circulation in the model. The top of the model is at 10 hPa, which may not be high enough to produce realistic circulation.

The comparison with surface observations highlights the advantage of an on-line model. The meteorological and transport signatures of ozone are well captured, but the climatological emissions used for this simulation do not capture any specific emission event which deviates from the general background values. In addition, our emissions are released into a 1.5°×1.5° grid square which for industrialized regions dilutes the NO_x emissions and makes for more efficient ozone generation, as in much of the domain the generation of ozone is NO_x-limited (Liu et al., 1987).

Overall, the comparison of carbon monoxide and nitrogen dioxide output with MOPITT and SCIAMACHY measurements emphasizes the need for more accurate, year-specific emissions rates for biomass burning and anthropogenic sources.

One of the means of characterising the general properties of an atmospheric model is via its OH oxidation capacity and for this two gases are generally useful, CH_4 and CH_3CCl_3 as their lifetimes can be characterised by other means. We have calculated their global chemical lifetimes, τ_i, using $\tau_i = \int n_i\, dz / \int k^i_{OH}\, n_i\, [OH]\, dz$ (averaged over a year) where n_i and [OH] represent the number densities of either CH_4 or CH_3CCl_3

---

[1] Lupu, A., Kaminski, J. W., Neary, L., McConnell, J. C., Jarosz, J., Rinsland, C., Bernath, P., Walker, K. A., Boone, C., O'Neill, N. T., Hyer, E. J., and Reid, J. S.: Alaskan and western Canadian wildfires in the summer of 2004: GEM-AQ simulations and comparison with ACE satellite measurements, to be submitted, 2007.

and OH, respectively and k^i_{OH} is the loss rate for the species with OH. Using the rate data from JPL 2003 we find τ_{CH_4} = 7.7 years and $\tau_{CH_3CCl_3}$ = 4.6 years to be compared with 8.4 years and 5.0 years, respectively from the IPCC report (IPCC, 2001). Another important metric for a tropospheric model is the flux of ozone from the stratosphere. We find that the flux of ozone through a single model layer with an average pressure of 200 hPa is 570 Tg/year. An amount of about 475 Tg (O_3)/yr is given in the IPCC report (2001) based on observed correlations with other gases (Murphy and Fahey, 1994; McLinden et al., 2000). In our simulations we have found that both the horizontal resolution and the use of the fully hybrid vertical co-ordinate system plays a significant role in the amounts of ozone coming down from the stratosphere. We found that using hybrid vertical coordinates reduced the ozone flux from the stratosphere by about 40% (based on 4°×4° simulations).

In the development of the model we have tried to be as internally consistent as possible when using transport information for the tracers: for example, for boundary layer transport we use the mixing coefficients from the physics module. However, for large scale convective transport we are using the Kuo scheme for the dynamics while using Zang-McFarlane for the tracers. We have commenced a study where we will use a Kain-Fritsch scheme modified for large scales for the dynamics, transport and lightning generation.

Acknowledgements. The authors wish to thank S. Gravel and colleagues at MSC for their assistance and advice with GEM and R. Sander for providing the MESSy photolysis module. The authors wish to acknowledge financial support from the Canadian Foundation for Climate and Atmospheric Sciences, Environment Canada, the Natural Sciences and Engineering Research Council of Canada, the Canadian Foundation for Innovation and the Ontario Innovation Trust. Also, we thank A. Hussain and M. Niesh for technical assistance.

References

Atkinson, R. and Lloyd, A. C.: Evaluation of kinetic and mechanistic data for modeling of photochemical smog, J. Phys. Chem. Ref. Data, 13, 315–444, 1984. 14926

Atkinson, R., Baulch, D. L., Cox, R. A., Hampson, Jr., R. F., Kerr, J. A., Rossi, M. J., and Troe, J.: Evaluated kinetic and photochemical for atmospheric chemistry, Organic Species: Supplement VII, IUPAC Subcommittee on Gas Kinetic Data Evaluation for Atmospheric Chemistry, J. Phys. Chem. Ref. Data, 28, 191–393, 1999. 14925

Atkinson, R., Baulch, D. L., Cox, R. A., Crowley, J. N., Hampson, R. F., Hynes, R. G., Jenkin, M. E., Rossi, M. J., and Troe, J.: Evaluated kinetic and photochemical data for atmospheric chemistry: Volume I - gas phase reactions of O_x, HO_x, NO_x and SO_x species, Atmos. Chem. Phys., 4, 1461–1738, 2004, http://www.atmos-chem-phys.net/4/1461/2004/. 14925

Atkinson, R., Baulch, D. L., Cox, R. A., Crowley, J. N., Hampson, R. F., Hynes, R. G., Jenkin, M. E., Rossi, M. J., and Troe, J.: Evaluated kinetic and photochemical data for atmospheric chemistry: Volume II - reactions of organic species, Atmos. Chem. Phys., 6, 3625–4055, 2005, http://www.atmos-chem-phys.net/6/3625/2005/. 14925

Benoît, R., Côté, J., and Méthot, A.: Inclusion of a TKE boundary layer parameterization in the Canadian Regional Finite-Element Model, Mon. Wea. Rev., 117, 1726–1750, 1989. 14899

Bovensmann, H., Burrows, J. P., Buchwitz, M., Frerick, J., Noël, S., Rozanov, V. V., Chance, K. V., and Goede, A. P. H.: SCIAMACHY: Mission objectives and measurement modes, J. Atmos. Sci., 56, 127–150, 1999. 14897, 14908

Burrows, J. P., Hölzle, E., Goede, A. P. H., Visser, H., and Fricke, W.: SCIAMACHY—Scanning imaging absorption spectrometer for atmospheric chartography, Acta Astronautica, 35, 445–451, 1995. 14897, 14908

Burrows, J. P., Weber, M., Buchwitz, M., Rozanov, V., Ladstätter-Weißenmayer, A., Richter, A., DeBeeka, R., Hoogena, R., Bramstedt, K., Eichmann, K.-U., Eisinger, M., and Perner, D.: The Global Ozone Monitoring Experiment (GOME): Mission concept and first scientific results, J. Atmos. Sci., 56, 151–175, 1999. 14897

Calvert, J. G. and Pitts, Jr., J. N.: Photochemistry, Wiley, New York, 1966. 14926

Côté, J., Desmarais, J.-G., Gravel, S., Méthot, A., Patoine, A., Roch, M., and Staniforth, A.: The operational CMC–MRB Global Environmental Multiscale (GEM) Model. Part II: Results, Mon. Wea. Rev., 126, 1397–1418, 1998a. 14896, 14898

Côté, J., Gravel, S., Méthot, A., Patoine, A., Roch, M., and Staniforth, A.: The operational

CMC–MRB Global Environmental Multiscale (GEM) Model. Part I: Design considerations and formulation, Mon. Wea. Rev., 126, 1373–1395, 1998b. 14898

de Grandpré, J., Beagley, S. R., Fomichev, V. I., Griffioen, E., McConnell, J. C., Medvedev, A. S., and Shepherd, T. G.: Ozone climatology using interactive chemistry: Results from the Canadian Middle Atmosphere Model, J. Geophys. Res., 105, 26 475–26 491, doi:10.1029/2000JD900427, 2000. 14900, 14903, 14908

Deardorff, J. W.: Efficient prediction of ground surface-temperature and moisture, with inclusion of a layer of vegetation, J. Geophys. Res., 83, 1889–1903, 1978. 14899

DeMore, W. B., Sander, S. P., Golden, D. M., Hampson, R. F., Kurylo, M. J., Howard, C. J., Ravishankara, A. R., Kolb, C. E., and Molina, M. J.: Chemical Kinetics and Photochemical Data for Use in Stratospheric Modeling, Evaluation 12, JPL Publication 97-4, Jet Propulsion Laboratory, Pasadena, California, 1997. 14926

Drummond, J. R.: Measurements of pollution in the troposphere (MOPITT), in: The use of EOS for studies of atmospheric physics, edited by Gille, J. C. and Visconti, G., pp. 77–101, North-Holland, 1992. 14897, 14906

Drummond, J. R. and Mand, G. S.: The Measurements of Pollution in the Troposphere (MOPITT) instrument: Overall performance and calibration requirements, J. Atmos. Ocean. Technol., 13, 314–320, 1996. 14897, 14906

Edwards, D. P., Pétron, G., Novelli, P. C., Emmons, L. K., Gille, J. C., and Drummond, J. R.: Southern Hemisphere carbon monoxide interannual variability observed by Terra/Measurement of Pollution in the Troposphere (MOPITT), J. Geophys. Res., 111, D16303, doi:10.1029/2006JD007079, 2006. 14907

Fishman, J., Hoell Jr., J. M., Bendura, R. D., McNeal, R. J., and Kirchhoff, V. W. J. H.: NASA GTE TRACE A Experiment (September–October 1992): Overview, J. Geophys. Res., 101, 23 865–23 880, doi:10.1029/96JD00123, 1996. 14897, 14909

Fouquart, Y. and Bonnel, B.: Computations of solar heating of the Earth's atmosphere: A new parameterization, Contrib. Atmos. Phys., 53, 35–62, 1980. 14899

Garand, L.: Some improvements and complements to the infrared emissivity algorithm including a parameterization of the absorption in the continuum region, J. Atmos. Sci., 40, 230–243, 1983. 14899

Garand, L. and Mailhot, J.: The influence of infrared radiation on numerical weather forecasts, in: Proceedings of the Seventh Conference on Atmospheric Radiation, July 23–27, 1990, San Francisco, CA, pp. J146–J151, Amer. Meteor. Soc., 1990. 14899

Gauthier, P., Charette, C., Fillion, L., Koclas, P., and Laroche, S.: Implementation of a 3D assimilation system at the Canadian Meteorological Centre. Part I: The global analysis., Atmos.-Ocean, 37, 103–156, 1999. 14903

Gauthier, P., Tanguay, M., Laroche, S., Pellerin, S., and Morneau, J.: Extension of 3D–Var to 4D–Var: implementation of 4D–Var at the Meteorological Service of Canada, Mon. Wea. Rev., 35, 2339–2354, 2007. 14903

Giguère, P. A. and Olmos, A. W.: Sur le spectre ultraviolet de l'acide peraéetique et l'hydrolyse des peracétates, Can. J. Chem., pp. 689–691, 1956. 14926

Gong, S. L., Barrie, L. A., Blanchet, J.-P., von Salzen, K., Lohmann, U., Lesins, G., Spacek, L., Zhang, L. M., Girard, E., Lin, H., Leaitch, R., Leighton, H., Chylek, P., and Huang, P.: Canadian Aerosol Module: A size-segregated simulation of atmospheric aerosol processes for climate and air quality models, 1. Module development, J. Geophys. Res., 108, 4007, doi:10.1029/2001JD002002, 2003. 14901

Gong, S. L., Huang, P., Zhao, T. L., Sahsuvar, L., Barrie, L. A., Kaminski, J. W., Li, Y. F., and Niu, T.: GEM/POPs: a global 3-D dynamic model for semi-volatile persistent organic pollutants - 1. Model description and evaluations, Atmos. Chem. Phys., 7, 4001–4013, 2007, http://www.atmos-chem-phys.net/7/4001/2007/. 14896

Grell, G. A., Peckham, S. E., Schmitz, R., McKeen, S. A., Frost, G., Skamarock, W. C., and Eder, B.: Fully coupled "online" chemistry within the WRF model, Atmos. Environ., 39, 6957–6975, 2005. 14897

Hervig, M. E., Russell III, J. M., Gordley, L. L., Park, J. H., and Drayson, S. R.: Observations of aerosol by the HALOE experiment onboard UARS: A preliminary validation, Geophys. Res. Lett., 20, 1291–1294, 1993. 14900

Horie, O. and Moortgat, G. K.: Reactions of CH3C(O)O2 radicals with CH3O2 and HO2 radicals between 263 and 333 K, J. Chem. Soc., Faraday Trans., 88, 3305–3312, 1992. 14925

Huang, P., Gong, S. L., Zhao, T. L., Neary, L., and Barrie, L. A.: GEM/POPs: a global 3-D dynamic model for semi-volatile persistent organic pollutants – Part 2: Global transports and budgets of PCBs, Atmos. Chem. Phys. Discuss., 7, 3837–3857, 2007, http://www.atmos-chem-phys-discuss.net/7/3837/2007/. 14896

IPCC: Climate Change 2001: The Scientific Basis. Contribution of Working Group I to the Third Assessment Report of the Intergovernmental Panel on Climate Change, Cambridge Univ. Press, New York, NY, USA, 2001. 14912

IUPAC: IUPAC Subcommittee on Gas Kinetic Data Evaluation for Atmospheric Chemistry, Data

Sheet NOx11, 19 July 2005, http://www.iupac-kinetic.ch.cam.ac.uk/, 2005a. 14925

IUPAC: IUPAC Subcommittee on Gas Kinetic Data Evaluation for Atmospheric Chemistry, Data Sheet HOx_VOC54, 17 February 2005, http://www.iupac-kinetic.ch.cam.ac.uk/, 2005b. 14925

IUPAC: IUPAC Subcommittee on Gas Kinetic Data Evaluation for Atmospheric Chemistry, Data Sheet HOx_VOC3, 5 December 2005, http://www.iupac-kinetic.ch.cam.ac.uk/, 2005c. 14925

IUPAC: IUPAC Subcommittee on Gas Kinetic Data Evaluation for Atmospheric Chemistry, Data Sheet HOx_VOC2, 21 July 2005, http://www.iupac-kinetic.ch.cam.ac.uk/, 2005d. 14925

IUPAC: IUPAC Subcommittee on Gas Kinetic Data Evaluation for Atmospheric Chemistry, Data Sheet HOx_VOC36, 21 July 2005, http://www.iupac-kinetic.ch.cam.ac.uk/, 2005e. 14925

IUPAC: IUPAC Subcommittee on Gas Kinetic Data Evaluation for Atmospheric Chemistry, Data Sheet ROO_1, 3 July 2005, http://www.iupac-kinetic.ch.cam.ac.uk/, 2005f. 14925

IUPAC: IUPAC Subcommittee on Gas Kinetic Data Evaluation for Atmospheric Chemistry, Data Sheet HOx_VOC23, 8 June 2005, http://www.iupac-kinetic.ch.cam.ac.uk/, 2005g. 14925

Jöckel, P., Tost, H., Pozzer, A., Brühl, C., Buchholz, J., Ganzeveld, L., Hoor, P., Kerkweg, A., Lawrence, M. G., Sander, R., Steil, B., Stiller, G., Tanarhte, M., Taraborrelli, D., van Aardenne, J., and Lelieveld, J.: The atmospheric chemistry general circulation model ECHAM5/MESSy1: consistent simulation of ozone from the surface to the mesosphere, Atmos. Chem. Phys., 6, 5067–5104, 2006, http://www.atmos-chem-phys.net/6/5067/2006/. 14897, 14901

Kaminski, J. W., Plummer, D. A., Neary, L., McConnell, J. C., Struzewska, J., and Lobocki, L.: First application of MC2-AQ to multiscale air quality modelling over Europe, Phys. Chem. Earth, 27, 1517–1524, 2002. 14897

Kuo, H. L.: Further studies on the parameterization of the influence of cumulus convection on largescale flow, J. Atmos. Sci., 31, 1232–1240, 1974. 14899

Landgraf, J. and Crutzen, P. J.: An efficient method for online calculations of photolysis and heating rates, J. Atmos. Sci., 55, 863–878, 1998. 14900

Langner, J., Robinson, L., Persson, C., and Ullerstig, A.: Validation of the operational emergency response model at the Swedish Meteorological and Hydrological Institute using data from ETEX and the Chernobyl accident - Description, test and sensitivity analysis in view of regulator applications, Atmos. Env., 32, 4325–4333, 1998. 14902

Laprise, R. and Girard, C.: A spectral general circulation model using a piecewise-constant finite-element representation on a hybrid vertical coordinate system, J. Climate, 3, 32–52,

1990. 14903

Laroche, S., Gauthier, P., Tanguay, M., Pellerin, S., and Morneau, J.: Impact of the different components of 4D–Var on the global forecast system of the Meteorological Service of Canada, Mon. Wea. Rev., 35, 2355–2364, 2007. 14903

Liu, S. C., Trainer, M., Fehsenfelf, F., Parrish, D. D., Williams, E. J., Fahey, D. W., Hubler, G., and Murphy, P. C.: Ozone production in the rural troposphere and the implications for regional and global ozone distribution, J. Geophys. Res., 92, 4191–4207, 1987. 14904, 14911

Liu, X., Chance, K., Sioris, C. E., Spurr, R. J. D., Kurosu, T. P., Martin, R. V., and Newchurch, M. J.: Ozone profile and tropospheric ozone retrievals from the Global Ozone Monitoring Experiment: Algorithm description and validation, J. Geophys. Res., 110, D20307, doi:10.1029/2005JD006240, 2005. 14905

Liu, X., Chance, K., Sioris, C. E., Kurosu, T. P., Spurr, R. J. D., Martin, R. V., Fu, M., Logan, J. A., Jacob, H. J., Palmer, P. I., Newchurch, M. J., Megretskaia, I., and Chatfield, R.: First directly retrieved global distribution of tropospheric column ozone from GOME: Comparison with the GEOS-CHEM model, J. Geophys. Res., 111, D02308, doi:10.1029/2005JD006564, 2006. 14905

Logan, J. A.: An analysis of ozonesonde data for the troposphere: Recommendations for testing 3-D models, and development of a gridded climatology for tropospheric ozone, J. Geophys. Res., 104, 16 115–16 149, 1999. 14897, 14904

Lurmann, F. W., Lloyd, A. C., and Atkinson, R.: A chemical mechanism for use in long-range transport/acid deposition computer modeling, J. Geophys. Res., 91, 10 905–10 936, 1986. 14900, 14926

Mailhot, J.: The regional finite-element (RFE) model scientific description. Part 2: Physics, Documentation Manual available from RPN, Meteorological Service of Canada, Dorval, QC, Canada, M9P 1J3, 1994. 14899

Mailhot, J., Chouinard, C., Benoît, R., Roch, M., and Verner, G.: Numerical forecasting of winter coastal storms during CASP - Evaluation of the regional finite-element model, Atmos.-Ocean., 27, 24–58, 1989. 14899

Marécal, V., Rivière, E. D., Held, G., Cautenet, S., and Freitas, S.: Modelling study of the impact of deep convection on the UTLS air composition – Part I: Analysis of ozone precursors, Atmos. Chem. Phys., 6, 1567–1584, 2006, http://www.atmos-chem-phys.net/6/1567/2006/. 14898

Martin, R. V., Sioris, C. E., Chance, K., Ryerson, T. B., Bertram, T. H., Wolldridge, P. J., Cohen,

R. C., Neuman, J. A., Swanson, A., and Flocke, F. M.: Evaluation of space-based constraints on global nitrogen oxide emissions with regional aircraft measurements over and downwind of eastern North America, J. Geophys. Res., 111, D15 308, doi:10.1029/2005JD006680, 2006. 14908

McFarlane, N. A.: The effect of orographically excited gravity wave drag on the general circulation of the lower stratosphere and troposphere, J. Atmos. Sci., 44, 1775–1800, 1987. 14899

McLandress, C. and McFarlane, N. A.: Interactions between orographic gravity wave drag and forced stationary planetary waves in the winter northern hemisphere middle atmosphere, J. Atmos. Sci., 50, 1966–1990, 1993. 14899

McLinden, C. A., Olsen, S. C., Hannegan, B., Wild, O., Prather, M. J., and Sundet, J.: Stratospheric ozone in 3-D models: A simple chemistry and the cross-tropopause flux, J. Geophys. Res., 105, 14 653–14 666, 2000. 14912

Molina, L. T. and Molina, M. J.: Absolute absorption cross sections of ozone in the 185- to 350-nm wavelength range, J. Geophys. Res., 91, 14 501–14 508, 1986. 14926

Murphy, D. M. and Fahey, D. W.: An estimate of the flux of stratospheric reactive nitrogen and ozone into the troposphere, J. Geophys. Res., 99, 5325–5332, 1994. 14912

Olivier, J. G. J. and Berdowski, J. J. M.: Global emissions sources and sinks, in: The Climate System, edited by: Guicherit, R. and Heij, B., pp. 33–78, A. A. Balkema Publishers/Swets and Zeitlinger Publishers, Lisse, The Netherlands, 2001. 14902

Olivier, J. G. J., Bouwman, A. F., Berdowski, J. J. M., Veldt, C., Bloos, J. P. J., Visschedijk, A. J. H., van der Maas, C. W. M., and Zandveld, P. Y. J.: Sectoral emission inventories of greenhouse gases for 1990 on a per country basis as well as on 1°×1°, Environ. Sci. Pol., 2, 241–263, 1999. 14902

O'Neill, N. T., Thulasiraman, S., Eck, T. F., and Reid, J. S.: Robust optical features of fine mode size distributions; application to the Québec smoke event of 2002, J. Geophys. Res., 110, D11207, doi:10.1029/2004JD005157, 2005. 14909

O'Neill, N. T., Campanelli, M., Lupu, A., Thulasiraman, S., Reid, J. S., Aubé, M., Neary, L., Kaminski, J. W., and McConnell, J. C.: Evaluation of the GEM–AQ air quality model during the Québec smoke event of 2002: Analysis of extensive and intensive optical disparities, Atmos. Environ., 40, 3737–3749, 2006. 14896

Pickering, K. E., Wang, Y., Tao, W.-K., Price, C., and Müller, J.-F.: Vertical distributions of lightning NO_x for use in regional and global chemical transport models, J. Geophys. Res., 103, 31 203–31 216, 1993. 14902

Plum, C. N., Atkinson, R., Carter, W. P. L., and Pitts, Jr., J. N.: OH radical rate constants and photolysis rates of α-dicarbonyls, Environ. Sci. Technol., 17, 479–484, 1983. 14926

Sander, S. P., Friedl, R. R., Golden, D. M., Kurylo, M. J., Moortgat, G. K., Keller-Rudek, H., Wine, P. H., Ravishankara, A. R., Kolb, C. E., Molina, M. J., Finlayson-Pitts, B. J., Huie, R. E., and Orkin, V. L.: Chemical Kinetics and Photochemical Data for Use in Atmospheric Studies, Evaluation Number 15, JPL Publication 06-2, Jet Propulsion Laboratory, 2006. 14925

Saunders, S. M., Jenkin, M. E., Derwent, R. G., and Pilling, M. J.: Protocol for the development of the Master Chemical Mechanism, MCM v3 (Part A): tropospheric degradation of non-aromatic volatile organic compounds, Atmos. Chem. Phys., 3, 161–180, 2003, http://www.atmos-chem-phys.net/3/161/2003/. 14925

Stockwell, W. R. and Lurmann, F. W.: Intercomparison of the ADOM and RADM Gas-Phase Chemistry Mechanisms. Report prepared for the Electric Power Research Institute, Electric Power Research Institute, 1989. 14925

Struzewska, J. and Kaminski, J. W.: Formation and transport of photooxidants over Europe during the July 2006 heat wave – observations and GEM–AQ model simulations, Atmos. Chem. Phys. Discuss., 7, 10 467–10 514, 2007. 14896, 14909

Talukdar, R. K., Longfellow, C. A., Gilles, M. K., and Ravishankara, A. R.: Quantum yields of O(^{1}D) in the photolysis of ozone between 289 and 329 nm as a function of temperature, Geophys. Res. Lett., 25, 143–146, 1998. 14926

Thompson, A. M., Witte, J. C., McPeters, R. D., Oltmans, S. J., Schmidlin, F. J., Logan, J. A., Fujiwara, M., Kirchhoff, V. W. J. H., Posny, F., Coetzee, G. J. R., Hoegger, B., Kawakami, S., Ogawa, T., Johnson, B. J., Vömel, H., and Labow, G.: Southern Hemisphere Additional Ozonesondes (SHADOZ) 1998-2000 tropical ozone climatology 1. Comparison with Total Ozone Mapping Spectrometer (TOMS) and ground-based measurements, J. Geophys. Res., 108, 8238, doi:10.1029/2001JD000967, 2003a. 14897, 14904

Thompson, A. M., Witte, J. C., Oltmans, S. J., Schmidlin, F. J., Logan, J. A., Fujiwara, M., Kirchhoff, V. W. J. H., Posny, F., Coetzee, G. J. R., Hoegger, B., Kawakami, S., Ogawa, T., Fortuin, J. P. F., and Kelder, H. M.: Southern Hemisphere Additional Ozonesondes (SHADOZ) 1998-2000 tropical ozone climatology 2. Tropospheric variability and the zonal wave-one, J. Geophys. Res., 108, 8241, doi:10.1029/2002JD002241, 2003b. 14897, 14904

Thornton, J. A., Braban, C. F., and Abbatt, J. P. D.: N2O5 hydrolysis on sub-micron organic aerosols: the effect of relative humidity, particle phase, and particle size, Phys. Chem. Chem.

Phys., 5, 4593–4603, 2003. 14925

Tulet, P., Crassier, V., Solmon, F., Guedalia, D., and Rosset, R.: Description of the Mesoscale Nonhydrostatic Chemistry model and application to a transboundary pollution episode between northern France and southern England, J. Geophys. Res., 108, 4021, doi:10.1029/2000JD000301, 2003. 14898

Venkatram, A., Karamchandani, P. K., and Misra, P. K.: Testing a comprehensive acid deposition model, Atmos. Environ., 22, 737–747, 1988. 14900

Wesely, M. L.: Parameterization of surface resistances to gaseous dry deposition in regional-scale numerical models, Atmos. Environ., 23, 1293–1304, 1989. 14901

Yeh, K.-S., Côté, J., Gravel, S., Méthot, A., Patoine, A., Roch, M., and Staniforth, A.: The CMC–MRB Global Environmental Multiscale (GEM) Model. Part III: Nonhydrostatic Formulation, Mon. Wea. Rev., 130, 339–356, 2002. 14899

Yu, W., Garand, L., and Dastoor, A. P.: Evaluation of model clouds and radiation at 100 km scale using GOES data, Tellus A, 49, 246, 1997. 14899

Zhang, G. J. and McFarlane, N. A.: Sensitivity of climate simulations to the parameterization of cumulus convection in the CCC-GCM, Atmos.-Ocean, 3, 407–446, 1995. 14900

Zhang, L., Moran, M. D., Makar, P. A., Brook, J. R., and Gong, S.: Modelling gaseous dry deposition in AURAMS: a unified regional air-quality modelling system, Atmos. Environ., 36, 537–560, 2002. 14901

Appendix A List of gas-phase chemistry in GEM-AQ

Table A1. List of gas-phase species.

No.	Species	
1	NO_2	Nitrogen dioxide
2	NO	Nitric oxide
3	HONO	Nitrous oxide
4	NO_3	Nitrate radical
5	N_2O_5	Dinitrogen pentoxide
6	HNO_4	Pernitric acid
7	HNO_3	Nitric acid
8	O_3	Ozone
9	H_2O_2	Hydrogen peroxide
10	SO_2	Sulphur dioxide
11	SO_4	Sulphate
12	O	Ground-state oxygen atom
13	$O(^1D)$	Exited-state oxygen atom
14	OH	Hydroxy radical
15	HO_2	Hydroperoxy radical
16	CO	Carbon monoxide
17	CH_4	Methane
18	C_2H_6	Ethane
19	C_3H_8	Propane and benzene
20	ALKA	Higher alkanes
21	ETHE	Ethene
22	ALKE	Higher alkenes
23	ISOP	Isoprene
24	TOLU	Toluene & other mono-substituted aromatics
25	CRES	o-Cresol
26	AROM	Xylene and other di- & tri-substituted aromatics
27	C_2H_2	Acetylene
28	HCHO	Formaldehyde
29	ALD2	Acetaldehyde and higher aldehydes
30	MEK	Acetone and higher ketones
31	MGLY	Glyoxal and methyl glyoxal
32	DIAL	Unsaturated di-carbonyls
33	PAN	Peroxyacetyl nitrate and higher PANs
34	RNO_3	Organic nitrate
35	ROOH	Organic peroxide
36	MOOH	Methyl hydroperoxide
37	MOH	Methanol
38	PAA	Peroxyacetic acid
39	FRMA	Formic acid
40	ACTA	Acetic acid
41	RO_2	Total RO_2 radicals (= RO_2R + R_2O_2 + RO_2N)
42	RO_2R	General organic peroxy radical #1
43	R_2O_2	General organic peroxy radical #2
44	RO_2N	Alkyl nitrate forming organic peroxy radical
45	MCO_3	Acetyl peroxy radical
46	MO_2	Methylperoxy radical
47	BZO	Phenoxy radical
48	CRG1	Criegee radical #1
49	CRG2	Criegee radical #2

Table A2. List of gas-phase reactions excluding those of sulphur chemistry in CAM.

No.	Reaction	Rate constant	Ref.
G001	$O + O_2 + M \rightarrow O_3 + M$	$k_0 = 1.57\times10^{-27}\,T^{-2.6}$	1.
G002	$O + NO_2 \rightarrow NO$	$k = 5.5\times10^{-12}\,\exp(188/T)$	1.
G003	$O + NO_2 + M \rightarrow NO_3 + M$	$k_0 = 6.75\times10^{-28}\,T^{-1.5}$ $k_\infty = 5.85\times10^{-12}\,T^{0.24}$ $F_c = 0.6$	1.
G004	$NO + O_3 \rightarrow NO_2$	$k = 1.4\times10^{-12}\,\exp(-1310/T)$	1.
G005	$NO_2 + O_3 \rightarrow NO_3$	$k = 1.4\times10^{-13}\,\exp(-2470/T)$	1.
G006	$NO + NO_3 \rightarrow NO_2 + NO_2$	$k = 1.8\times10^{-11}\,\exp(110/T)$	1.
G007	$NO + NO\ (+ O_2) \rightarrow NO_2 + NO_2$	$k = 3.3\times10^{-39}\,\exp(530/T)\times[M]\times0.21$	1.
G008	$NO_2 + NO_3 + M \rightarrow N_2O_5 + M$	$k_0 = 1.59\times10^{-19}\,T^{-4.4}$ $k_\infty = 7.59\times10^{-11}\,T^{-0.7}$ $F_c = 0.6$	2.
G009	$N_2O_5 + M \rightarrow NO_2 + NO_3 + M$	$k_{uni} = 3.7\times10^{26}\,\exp(-11000/T)\times k_{G008}$	2.
G010	$N_2O_5 + H_2O \rightarrow 2\,HNO_3$	$k = 2.5\times10^{-22} + 1.8\times10^{-39}\times[H_2O]$	1.
G011	$NO_2 + NO_3 \rightarrow NO + NO_2$	$k = 4.5\times10^{-14}\,\exp(-1260/T)$	2.
G012	$O(^1D) + H_2O \rightarrow 2\,OH$	$k = 2.2\times10^{-10}$	1.
G013	$O(^1D) + M \rightarrow O + M$	$k = 0.78\times1.8\times10^{-11}\,\exp(107/T)$ $+0.21\times3.2\times10^{-11}\,\exp(67/T)$	1.
G014	$NO + OH + M \rightarrow HONO + M$	$k_0 = 6.52\times10^{-25}\,T^{-2.4}$ $k_\infty = 1.83\times10^{-10}\,T^{-0.3}$ $F_c = 0.81$	1.
G015	$NO_2 + NO_2 + H_2O \rightarrow HNO_3 + HONO$	$k = 1.0\times10^{-24}$	3
G016	$NO_2 + OH + M \rightarrow HNO_3 + M$	$k_0 = 8.91\times10^{-23}\,T^{-3.0}$ $k_\infty = 4.1\times10^{-11}$ $F_c = 0.4$	1.
G017	$HNO_3 + OH \rightarrow NO_3$	$k = k_1 + k_2[M]/(1 + k_2[M]/k_3)$ $k_1 = 2.4\times10^{-14}\,\exp(460/T)$ $k_2 = 6.5\times10^{-34}\,\exp(1335/T)$ $k_3 = 2.7\times10^{-17}\,\exp(2199/T)$	1.
G018	$CO + OH \rightarrow HO_2$	$k = 1.44\times10^{-13}\times(1 + [M]/(4.2\times10^{19}))$	4.
G019	$OH + O_3 \rightarrow HO_2$	$k = 1.7\times10^{-12}\,\exp(-940/T)$	1.
G020	$NO + HO_2 \rightarrow NO_2 + OH$	$k = 3.6\times10^{-12}\,\exp(270/T)$	1.
G021	$HO_2 + NO_2 + M \rightarrow HNO_4 + M$	$k_0 = 5.29\times10^{-23}\,T^{-3.4}$ $k_\infty = 1.54\times10^{-9}\,T^{-1.1}$ $F_c = 0.6$	2.
G022	$HNO_4 + M \rightarrow NO_2 + HO_2 + M$	$k_{uni} = 4.76\times10^{26}\,\exp(-10900/T)\times k_{G021}$	2.
G023	$HNO_4 + OH \rightarrow NO_2$	$k = 3.2\times10^{-13}\,\exp(690/T)$	5.
G024	$HO_2 + O_3 \rightarrow OH$	$k = 9.71\times10^{-28}\,T^{4.57}\,\exp(693/T)$	1.
G025	$HO_2 + HO_2 \rightarrow H_2O_2$	$k = 2.2\times10^{-13}\,\exp(600/T)$	1.
G026	$HO_2 + HO_2 + M \rightarrow H_2O_2 + M$	$k_0 = 1.9\times10^{-33}\,\exp(980/T)$	1.
G027	$HO_2 + HO_2 \rightarrow H_2O_2$	$k = 3.08\times10^{-34}\,\exp(2800/T)[H_2O]$	1.
G028	$HO_2 + HO_2 + M \rightarrow H_2O_2 + M$	$k_0 = 2.66\times10^{-54}\,\exp(3180/T)[H_2O]$	1.
G029	$H_2O_2 + OH \rightarrow HO_2$	$k = 2.9\times10^{-12}\,\exp(-160/T)$	1.
G030	$HO_2 + NO_3 \rightarrow OH + NO_2$	$k = 4.0\times10^{-12}$	1.
G031	$SO_2 + OH + M \rightarrow SO_4 + HO_2 + M$	$k = 0.0$ (Handled in aerosol module)	
G032	$RO_2 + NO \rightarrow NO$	$k = 4.2\times10^{-12}\,\exp(180/T)$	3.
G033	$RO_2 + HO_2 \rightarrow HO_2$	$k = 1.75\times10^{-13}\,\exp(1000/T)$	3.
G034	$RO_2 + RO_2 \rightarrow$	$k = 1.0\times10^{-15}$	3.
G035	$RO_2 + MCO_3 \rightarrow MCO_3$	$k = 3.0\times10^{-12}$	3.
G036	$HCHO + OH \rightarrow CO + HO_2$	$k = 5.4\times10^{-12}\,\exp(135/T)$	4.
G037	$HCHO + NO_3 \rightarrow HNO_3 + CO + HO_2$	$k = 5.6\times10^{-16}$	4 .
G038	$HCHO + HO_2 \rightarrow RO_2 + RO_2R$	$k = k_1\times(1 - 1/A)$ $k_1 = 1.1\times10^{-13}$ $A = 1 + 2.1\times10^{-19}\,\exp(180/T)\,\chi_{NO}(ppmv)\,[M]$	3.

Title Page
Abstract | Introduction
Conclusions | References
Tables | Figures
◀| |▶
◀ ▶
Back | Close
Full Screen / Esc
Printer-friendly Version
Interactive Discussion

Table A2. Continued.

No.	Reaction	Rate constant	Ref.
G039	$\mathrm{ALD2 + OH \rightarrow MCO_3}$	$k = 4.4\times10^{-12}\exp(365/T)$	4.
G040	$\mathrm{ALD2 + NO_3 \rightarrow HNO_3 + MCO_3}$	$k = 1.4\times10^{-12}\exp(-1860/T)$	4.
G041	$\mathrm{MCO_3 + NO \rightarrow MO_2 + NO_2}$	$k = 7.5\times10^{-12}\exp(290/T)$	4.
G042	$\mathrm{MCO_3 + NO_2 + M \rightarrow PAN + M}$	$k_0 = 7.22\times10^{-15}\,T^{-5.6}$ $k_\infty = 4.83\times10^{-8}\,T^{-1.5}$ $F_c = 0.6$	2.
G043	$\mathrm{MCO_3 + HO_2 \rightarrow \alpha_1\ PAA + \alpha_2\ ACTA + \alpha_2\ O_3}$	$k = 5.2\times10^{-13}\exp(980/T)$ $\alpha_1 = 1 - \alpha_2$ $\alpha_2 = \min(1.0,\ 8.5\times10^{-3}\exp(1020/T))$	6. 7., 8.
G044	$\mathrm{MCO_3 + MCO_3 \rightarrow 2\ MO_2}$	$k = 2.9\times10^{-12}\exp(500/T)$	4.
G045	$\mathrm{PAN + M \rightarrow NO_2 + MCO_3 + M}$	$k_{\mathrm{uni}} = 1.11\times10^{28}\exp(-14000/T)\times k_{\mathrm{G042}}$	2.
G046	$\mathrm{MEK + OH \rightarrow 0.5\ HCHO + 0.5\ ALD2 + 1.5\ RO_2}$ $\mathrm{+\ 1.5\ RO_2R + MCO_3}$	$k = 1.2\times10^{-11}\exp(-745/T)$	3.
G047	$\mathrm{MGLY + OH \rightarrow CO + MCO_3}$	$k = 1.5\times10^{-11}$	4.
G048	$\mathrm{MGLY + NO_3 \rightarrow HNO_3 + CO + MCO_3}$	$k = 3.0\times10^{-13}\exp(-1427/T)$	3.
G049	$\mathrm{CH_4 + OH \rightarrow MO_2}$	$k = 2.8\times10^{-14}\,T^{0.667}\exp(-1575/T)$	2.
G050	$\mathrm{C_2H_6 + OH \rightarrow ALD2 + RO_2 + RO_2R}$	$k = 6.9\times10^{-12}\exp(-1000/T)$	4.
G051	$\mathrm{C_3H_8 + OH \rightarrow 0.3\ ALD2 + 0.5\ MEK + RO_2 + RO_2R}$	$k = 1.65\times10^{-17}\,T^2\exp(-87/T)$	4.
G052	$\mathrm{ALKA + OH \rightarrow \beta_{pt(1)}\ HCHO + \beta_{pt(2)}\ ALD2}$ $\mathrm{+\ \beta_{pt(3)}\ MEK + \beta_{pt(4)}\ RO_2N}$ $\mathrm{+\ \beta_{pt(5)}\ RO_2R + \beta_{pt(6)}\ R_2O_2 + \beta_{pt(7)}\ RO_2}$	$k = X\,k_1 + (1 - X)\,k_2$ $k_1 = 1.017\times10^{-11}\exp(-354/T)$ $k_2 = 2.312\times10^{-11}\exp(-289/T)$	3.
G053	$\mathrm{RNO_3 + OH \rightarrow 0.16\ HCHO + 1.53\ ALD2 + 0.15\ MEK}$ $\mathrm{+\ NO_2 + 1.39\ RO_2 + 1.39\ R_2O_2}$	$k = 2.19\times10^{-11}\exp(-709/T)$	3.
G054	$\mathrm{RO_2N + NO \rightarrow RNO_3}$	$k = 4.2\times10^{-12}\exp(180/T)$	3.
G055	$\mathrm{RO_2N + HO_2 \rightarrow MEK + ROOH}$	$k = 1.75\times10^{-13}\exp(1000/T)$	3.
G056	$\mathrm{RO_2N + RO_2 \rightarrow MEK + 0.5\ HO_2 + RO_2}$	$k = 1.0\times10^{-15}$	3.
G057	$\mathrm{RO_2N + MCO_3 \rightarrow 0.7\ MO_2 + 0.7\ HO_2 + 0.3\ ACTA + MEK}$	$k = 3.0\times10^{-12}$	3., 9.
G058	$\mathrm{R_2O_2 + NO \rightarrow NO_2}$	$k = 4.2\times10^{-12}\exp(180/T)$	3.
G059	$\mathrm{R_2O_2 + HO_2 \rightarrow ROOH}$	$k = 1.75\times10^{-13}\exp(1000/T)$	3.
G060	$\mathrm{R_2O_2 + RO_2 \rightarrow RO_2}$	$k = 1.0\times10^{-15}$	3
G061	$\mathrm{R_2O_2 + MCO_3 \rightarrow 0.7\ MO_2 + 0.3\ ACTA}$	$k = 3.0\times10^{-12}$	3., 9.
G062	$\mathrm{RO_2R + NO \rightarrow NO_2 + HO_2}$	$k = 4.2\times10^{-12}\exp(180/T)$	3.
G063	$\mathrm{RO_2R + HO_2 \rightarrow ROOH}$	$k = 1.75\times10^{-13}\exp(1000/T)$	3.
G064	$\mathrm{RO_2R + RO_2 \rightarrow 0.5\ HO_2 + RO_2}$	$k = 1.0\times10^{-15}$	3.
G065	$\mathrm{RO_2R + MCO_3 \rightarrow 0.7\ MO_2 + 0.7\ HO_2 + 0.3\ ACTA}$	$k = 3.0\times10^{-12}$	3., 9.
G066	$\mathrm{ETHE + OH \rightarrow 1.56\ HCHO + 0.22\ ALD2 + RO_2 + RO_2R}$	$k_0 = 4.11\times10^{-21}\,T^{-3.1}$ $k_\infty = 1.15\times10^{-9}\,T^{-0.85}$ $F_c = 0.48$	10.
G067	$\mathrm{ETHE + O_3 \rightarrow HCHO + 0.42\ CO + 0.4\ CRG1 + 0.12\ HO_2}$	$k = 9.1\times10^{-15}\exp(-2580/T)$	4.
G068	$\mathrm{ETHE + O \rightarrow HCHO + CO + HO_2 + RO_2 + RO_2R}$	$k = 1.04\times10^{-11}\exp(-792/T)$	3.
G069	$\mathrm{ETHE + NO_3 \rightarrow 2\ HCHO + NO_2 + RO_2 + R_2O_2}$	$k = 3.3\times10^{-12}\exp(-2880/T)$	4.
G070	$\mathrm{ALKE + OH \rightarrow \beta_{c(1)}\ HCHO + \beta_{c(2)}\ ALD2 + RO_2 + RO_2R}$	$k = Y\,k_1 + (1 - Y)\,k_2$ $k_1 = 5.323\times10^{-12}\exp(504/T)$ $k_2 = 1.074\times10^{-11}\exp(549/T)$	3.
G071	$\mathrm{ALKE + O_3 \rightarrow \beta_{c(3)}\ HCHO + \beta_{c(4)}\ ALD2 + \beta_{c(5)}\ RO_2}$ $\mathrm{+\ \beta_{c(5)}\ RO_2R + \beta_{c(6)}\ HO_2 + \beta_{c(7)}\ OH}$ $\mathrm{+\ \beta_{c(8)}\ CO + \beta_{c(18)}\ CRG1 + \beta_{c(19)}\ CRG2}$	$k = Y\,k_1 + (1 - Y)\,k_2$ $k_1 = 1.323\times10^{-14}\exp(-2105/T)$ $k_2 = 7.333\times10^{-15}\exp(-1137/T)$	3.
G072	$\mathrm{ALKE + O \rightarrow \beta_{c(9)}\ CO + \beta_{c(10)}\ MEK + \beta_{c(11)}\ HCHO}$ $\mathrm{+\ \beta_{c(12)}\ ALD2 + \beta_{c(13)}\ HO_2 + \beta_{c(14)}\ RO_2}$ $\mathrm{+\ \beta_{c(14)}\ RO_2R}$	$k = Y\,k_1 + (1 - Y)\,k_2$ $k_1 = 1.18\times10^{-11}\exp(-324/T)$ $k_2 = 2.26\times10^{-11}\exp(10/T)$	3.
G073	$\mathrm{ALKE + NO_3 \rightarrow \beta_{c(1)}\ HCHO + \beta_{c(2)}\ ALD2 + NO_2 + RO_2}$ $\mathrm{+\ R_2O_2}$	$k = Y\,k_1 + (1 - Y)\,k_2$ $k_1 = 1.143\times10^{-11}\exp(-1935/T)$ $k_2 = 3.23\times10^{-11}\exp(-975/T)$	3.

Table A2. Continued.

No.	Reaction	Rate constant	Ref.
G076	$CRG1 + H_2O \rightarrow FRMA$	$k = 2.3\times10^{-17}$	3.
G077	$CRG2 + H_2O \rightarrow ACTA$	$k = 2.3\times10^{-17}$	3.
G078	$HCHO + CRG1 \rightarrow$	$k = 2.5\times10^{-14}$	3.
G079	$HCHO + CRG2 \rightarrow$	$k = 2.5 \times 10^{-14}$	3.
G080	$ALD2 + CRG1 \rightarrow$	$k = 2.5\times10^{-14}$	3.
G081	$ALD2 + CRG2 \rightarrow$	$k = 2.5\times10^{-14}$	3.
G082	$TOLU + OH \rightarrow 0.11\ HCHO + 0.14\ MGLY + 0.4\ DIAL + 0.11\ CO + 0.16\ CRES + 0.16\ HO_2 + 0.84\ RO_2 + 0.84\ RO_2R$	$k = 2.1\times10^{-12} \exp(322/T)$	3.
G083	$AROM + OH \rightarrow \beta_{c(15)}\ DIAL + \beta_{c(16)}\ MGLY + \beta_{c(17)}\ HCHO + \beta_{c(17)}\ CO + 0.17\ CRES + 0.17\ HO_2 + 0.83\ RO_2 + 0.83\ RO_2R$	$k = Z\,k_1 + (1-Z)\,k_2$ $k_1 = 1.407\times10^{-11} \exp(116/T)$ $k_2 = 4.77\times10^{-11}$	3.
G084	$DIAL + OH \rightarrow MCO_3$	$k = 3.0\times10^{-11}$	3.
G085	$CRES + OH \rightarrow 0.2\ MGLY + 0.08\ CRES + RO_2 + 0.85\ RO_2R + 0.15\ RO_2N$	$k = 4.0\times10^{-11}$	3.
G086	$CRES + NO_3 \rightarrow HNO_3 + BZO + 0.5\ CRES$	$k = 2.2\times10^{-11}$	3.
G087	$BZO + NO_2 \rightarrow RNO_3$	$k = 1.5\times10^{-11}$	3.
G088	$BZO + HO_2 \rightarrow$	$k = 1.75\times10^{-13} \exp(1000/T)$	3.
G089	$BZO \rightarrow$	$k_{uni} = 1.0\times10^{-3}$	3.
G090	$ISOP + OH \rightarrow ETHE + HCHO + 0.2\ ALD2 + 0.27\ MGLY + 0.7\ HO_2 + RO_2 + 0.9\ R_2O_2 + 0.2\ MCO_3 + 0.1\ RO_2N$	$k = 2.7\times10^{-11} \exp(390/T)$	4.
G091	$ISOP + O_3 \rightarrow 0.5\ ETHE + HCHO + 0.4\ ALD2 + 0.2\ MGLY + 0.2\ CRG2 + 0.4\ HO_2 + 0.1\ OH$	$k = 1.03\times10^{-14} \exp(-1995/T)$	4.
G092	$ISOP + O \rightarrow ETHE + ALD2 + 0.6\ HO_2 + 0.5\ RO_2 + 0.5\ R_2O_2$	$k = 1.8\times10^{-11}$	3.
G093	$ISOP + NO_3 \rightarrow HCHO + ALD2 + NO_2 + RO_2 + R_2O_2$	$k = 3.15\times10^{-12} \exp(-450/T)$	4.
G094	$OH + HO_2 \rightarrow$	$k = 4.8\times10^{-11} \exp(250/T)$	1.
G095	$ROOH + OH \rightarrow 0.5\ OH + 0.5\ RO_2 + 0.5\ RO_2R$	$k = 4.0\times10^{-12} \exp(180/T)$	3.
G096	$C_2H_2 + OH + M \rightarrow$	$k_0 = 2.6\times10^{-26}\,T^{-1.5}$ $k_\infty = 1.0\times10^{-12}$ $F_c = 0.37$	11.
G097	$RO_2N + MO_2 \rightarrow 0.75\ HCHO + 0.25\ MOH + HO_2 + MEK$	$k = 1.0\times10^{-15}$	$= k_{\mathrm{G056}}$
G098	$RO_2N + NO_3 \rightarrow NO_2 + HO_2 + MEK$	$k = 2.5\times10^{-12}$	9.
G099	$R_2O_2 + MO_2 \rightarrow 0.5\ HCHO + 0.5\ MO_2$	$k = 1.0\times10^{-15}$	$= k_{\mathrm{G060}}$
G100	$R_2O_2 + NO_3 \rightarrow NO_2$	$k = 2.5\times10^{-12}$	9.
G101	$RO_2 + MO_2 \rightarrow MO_2$	$k = 1.0\times10^{-15}$	$= k_{\mathrm{G034}}$
G102	$RO_2 + NO_3 \rightarrow NO_3$	$k = 2.5\times10^{-12}$	9.
G103	$RO_2R + MO_2 \rightarrow HO_2 + 0.75\ HCHO + 0.25\ MO_2$	$k = 1.0\times10^{-15}$	$= k_{\mathrm{G064}}$
G104	$RO_2R + NO_3 \rightarrow NO_2 + HO_2$	$k = 2.5\times10^{-12}$	9.
G105	$MCO_3 + NO_3 \rightarrow MO_2 + NO_2$	$k = 4.1\times10^{-12}$	9.
G106	$PAN + OH \rightarrow HCHO + CO + NO_2$	$k = 2.0\times10^{-14}$	4.
G107	$FRMA + OH \rightarrow HO_2$	$k = 4.5\times10^{-13}$	4.
G108	$ACTA + OH \rightarrow MO_2$	$k = 4.2\times10^{-14} \exp(855/T)$	12.
G109	$MO_2 + NO \rightarrow NO_2 + HCHO + HO_2$	$k = 2.3\times10^{-12} \exp(360/T)$	13.
G110	$MO_2 + HO_2 \rightarrow MOOH$	$k = 3.8\times10^{-13} \exp(780/T)$	4.
G111	$MO_2 + MO_2 \rightarrow 2\ HCHO + 2\ HO_2$	$k = 7.4\times10^{-13} \exp(-520/T)$	4.
G112	$MO_2 + MO_2 \rightarrow HCHO + MOH$	$k = 1.03\times10^{-13} \exp(365/T) - k_{\mathrm{G111}}$	4.
G113	$MO_2 + MCO_3 \rightarrow HCHO + \alpha_3\ HO_2 + \alpha_3\ MO_2 + \alpha_4\ ACTA$	$k = 2.0\times10^{-12} \exp(500/T)$ $\alpha_3 = 1 - \alpha_4$ $\alpha_4 = \min(1.0,\ 6.1\times10^{-6} \exp(2990/T))$	4. 7., 8.
G114	$MO_2 + NO_3 \rightarrow NO_2 + HCHO + HO_2$	$k = 1.3\times10^{-12}$	4.

Table A2. Continued.

No.	Reaction	Rate constant	Ref.
G115	$MOOH + OH \rightarrow 0.65\ MO_2 + 0.35\ HCHO + 0.35\ OH$	$k = 2.9\times10^{-12}\exp(190/T)$	4.
G116	$MOH + OH \rightarrow HCHO + HO_2$	$k = 2.85\times10^{-12}\exp(-345/T)$	14.
G117	$PAA + OH \rightarrow MCO_3$	$k = 3.7\times10^{-12}$	9.
G118	$N_2O_5 + H_2O \rightarrow 2\ HNO_3$	$\gamma = \begin{cases} 0.001 + 0.068\,RH & (0 \le RH < 0.5) \\ 0.035 & (0.5 \le RH \le 1) \end{cases}$	15.

References:
1. Atkinson et al. (2004);
2. Sander et al. (2006);
3. Stockwell and Lurmann (1989);
4. Atkinson et al. (2005);
5. IUPAC (2005a);
6. IUPAC (2005b);
7. Atkinson et al. (1999);
8. Horie and Moortgat (1992);
9. Saunders et al. (2003);
10. IUPAC (2005c);
11. IUPAC (2005d);
12. IUPAC (2005e);
13. IUPAC (2005f);
14. IUPAC (2005g);
15. Thornton et al. (2003).

Table A3. List of photolysis reactions.

No.	Reaction	Ref.
P01	$NO_2 + h\nu \rightarrow NO + O$	1.
P02	$NO_3 + h\nu \rightarrow NO$	1.
P03	$NO_3 + h\nu \rightarrow NO_2 + O$	1.
P04	$O_3 + h\nu \rightarrow O$	2., 3.
P05	$O_3 + h\nu \rightarrow O(^1D)$	2., 3.
P06	$HONO + h\nu \rightarrow NO + OH$	1.
P07	$HNO_3 + h\nu \rightarrow NO_2 + OH$	1.
P08	$HNO_4 + h\nu \rightarrow NO_2 + HO_2$	1.
P09	$H_2O_2 + h\nu \rightarrow 2\ OH$	1.
P10	$ROOH + h\nu \rightarrow HO_2 + OH$	$= J_{P17}$
P11	$HCHO + h\nu \rightarrow CO + 2.\ HO_2$	1.
P12	$HCHO + h\nu \rightarrow CO$	1.
P13	$ALD2 + h\nu \rightarrow MO_2 + CO + HO_2$	4., 5.
P14	$MEK + h\nu \rightarrow ALD2 + RO_2 + RO_2R + MCO_3$	6.
P15	$MGLY + h\nu \rightarrow CO + HO_2 + MCO_3$	7.
P16	$DIAL + h\nu \rightarrow CO + HO_2 + MCO_3$	8., $= J_{P01} \times 0.005$
P17	$MOOH + h\nu \rightarrow HCHO + HO_2 + OH$	1.
P18	$PAA + h\nu \rightarrow MO_2 + OH$	9.
P19	$PAN + h\nu \rightarrow MCO_3 + NO_2$	1.

References for absorption cross sections and quantum yields:

1. DeMore et al. (1997);
2. Molina and Molina (1986);
3. Talukdar et al. (1998);
4. Calvert and Pitts (1966);
5. Atkinson and Lloyd (1984);
6. Crowley, J. N., unpublished data;
7. Plum et al. (1983);
8. Lurmann et al. (1986);
9. Giguère and Olmos (1956).

Table A4. Emissions. All VOC emissions are given in TgC/year, NO and NO_2 in TgN/year, SO_2 in TgS/year, and CO in TgCO/year.

Species	Industrial	Biogenic	Fuelwood and agricultural waste burning	Forest and savannah burning	Lightning
C3H8	5.0	2.7	0.96	1.6	
TOLU	4.1				
AROM	6.8	138.9	15.7	4.1	
ETHE	2.0	12.6	4.8	9.2	
HCHO	0.25				
MEK	0.7				
ALD2	0.34				
ALKA	38.4	111.1	12.5	3.3	
CO	306.7	19.9	377.6	470.4	
C2H6	3.2	1.6	2.45	2.96	
ISOP		501.0			
ALKE		27.3	3.1	0.82	
NO	21.9	6.6	3.5	6.5	2.0
NO2	1.15				
SO2	71.6				

Title Page
Abstract
Introduction
Conclusions
References
Tables
Figures
◀◀
▶▶
◀
▶
Back
Close
Full Screen / Esc
Printer-friendly Version
Interactive Discussion

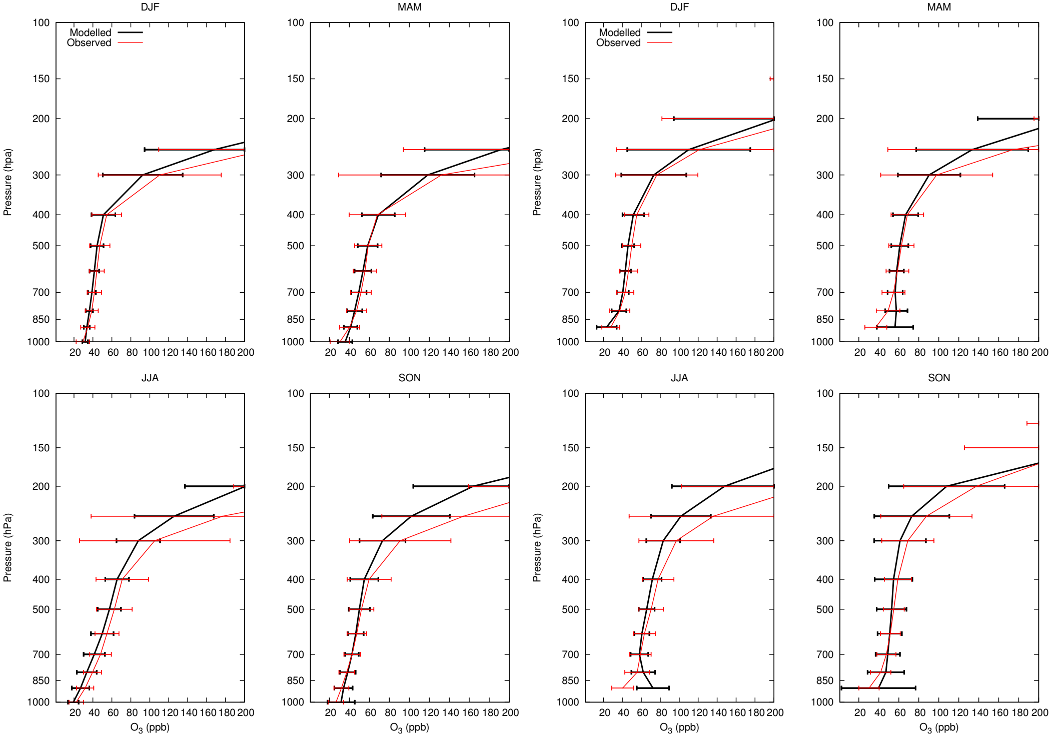

Fig. 1. Seasonal comparison of GEM-AQ and ozonesonde climatology for **(a)** Churchill and **(b)** Hohenpeissenberg stations.

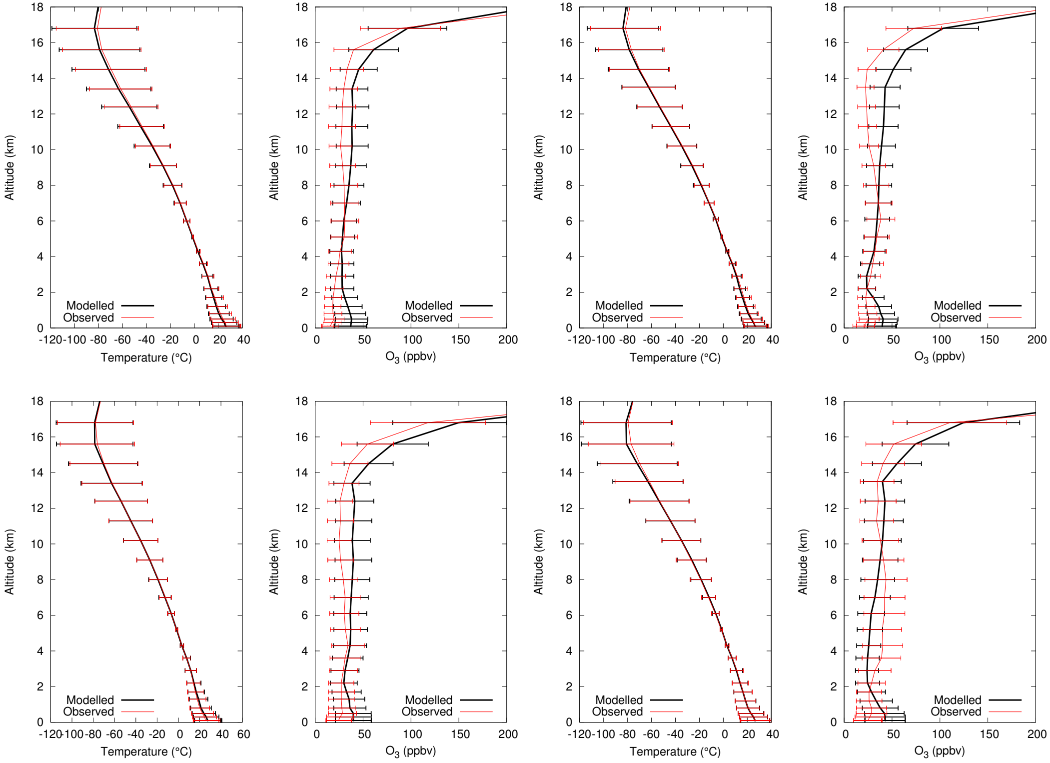

Fig. 2. Seasonally averaged ozone profiles for South Pacific stations (Fiji, Kuala Lumpur, Samoa and Watukosek), 2001: **(a)** DJF **(b)** MAM **(c)** JJA **(d)** SON.

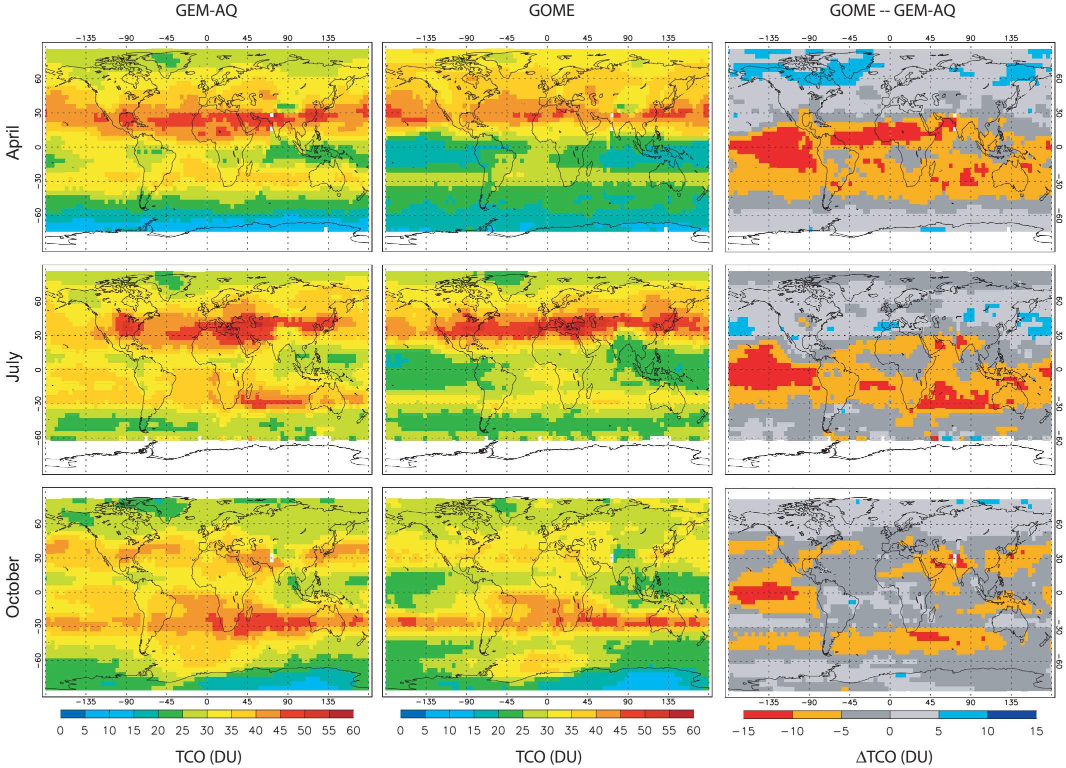

Fig. 3. GEM-AQ, GOME and GOME–GEM differences of tropospheric column ozone for April, July and October, 2001.

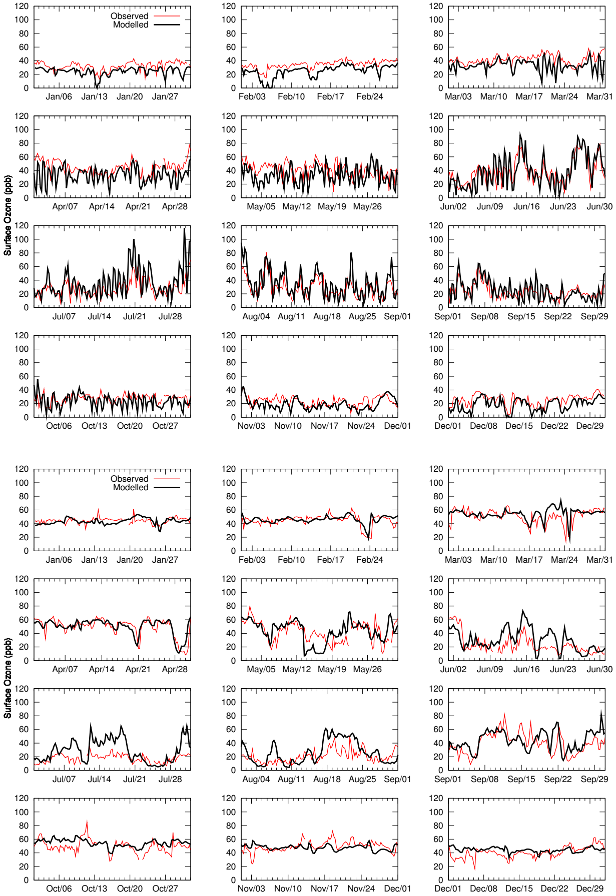

Fig. 4. 2001 surface ozone timeseries for Algoma, Canada **(a)** and Yonagunijima, Japan **(b)**.

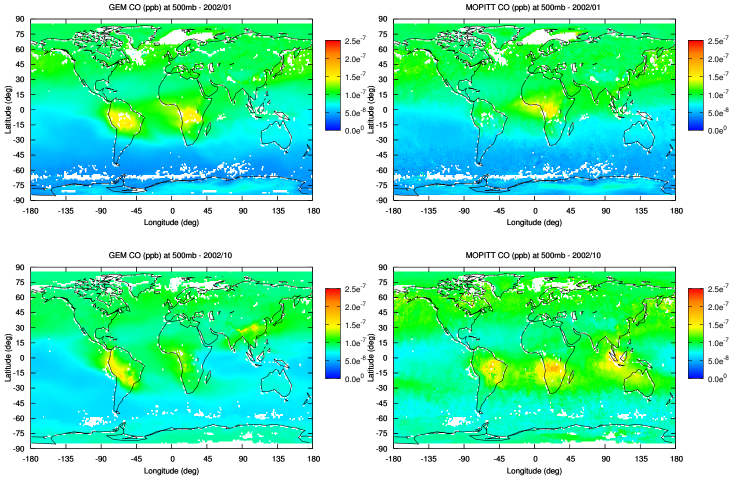

Fig. 5. GEM-AQ and MOPITT CO at 500 hPa for January and October 2002. Only cloud-free pixels are shown.

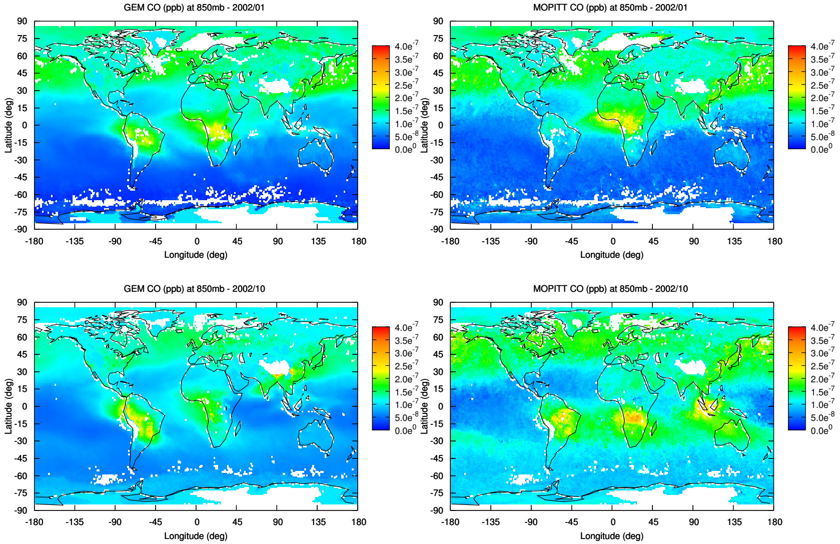

Fig. 6. GEM-AQ and MOPITT CO at 850 hPa for January and October 2002. Only cloud-free pixels are shown.

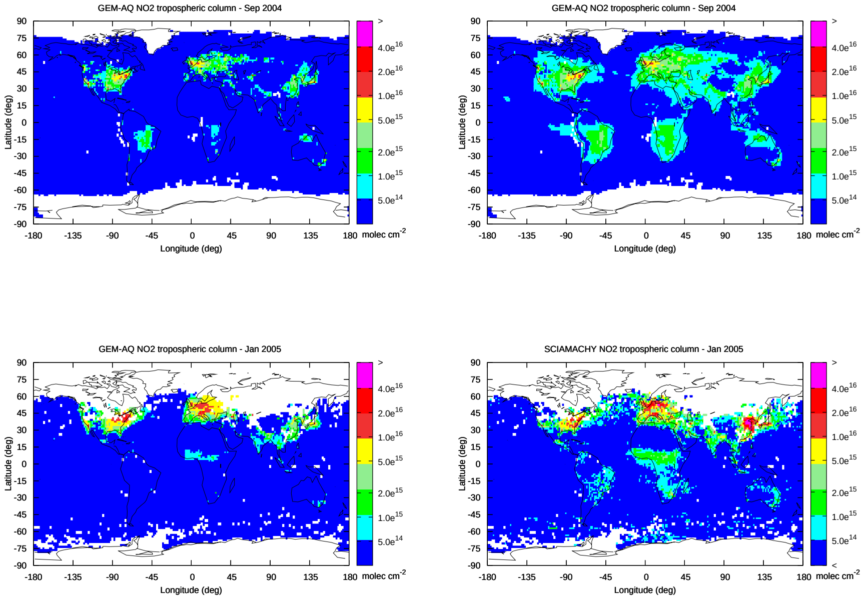

Fig. 7. September 2004 tropospheric NO2 column from **(a)** GEM-AQ using the subtraction of the Pacific sector and **(b)** SCIAMACHY. Figures **(c)** and **(d)** are for January 2005.

Title Page
Abstract
Introduction
Conclusions
References
Tables
Figures
◀◀
▶▶
◀
▶
Back
Close
Full Screen / Esc
Printer-friendly Version
Interactive Discussion

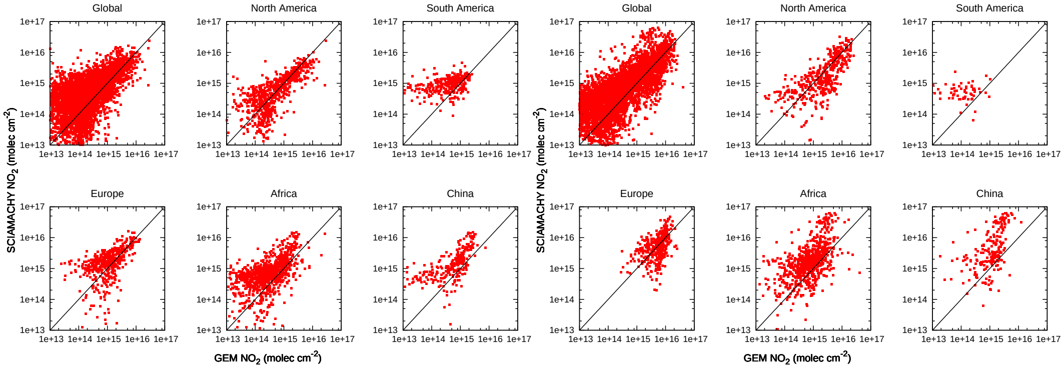

Fig. 8. GEM-AQ vs. SCIAMACHY tropospheric NO_2 column correlations for **(a)** September 2004 and **(b)** January 2005.

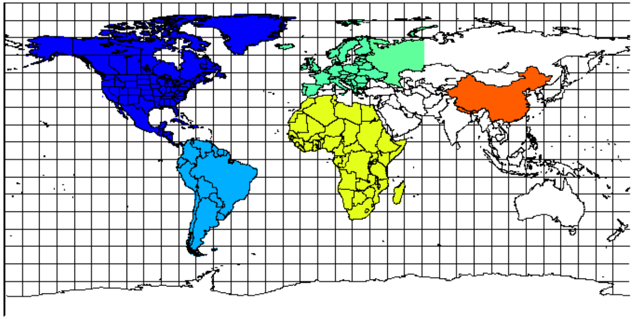

Fig. 9. Regions used for correlations in Fig. 8.

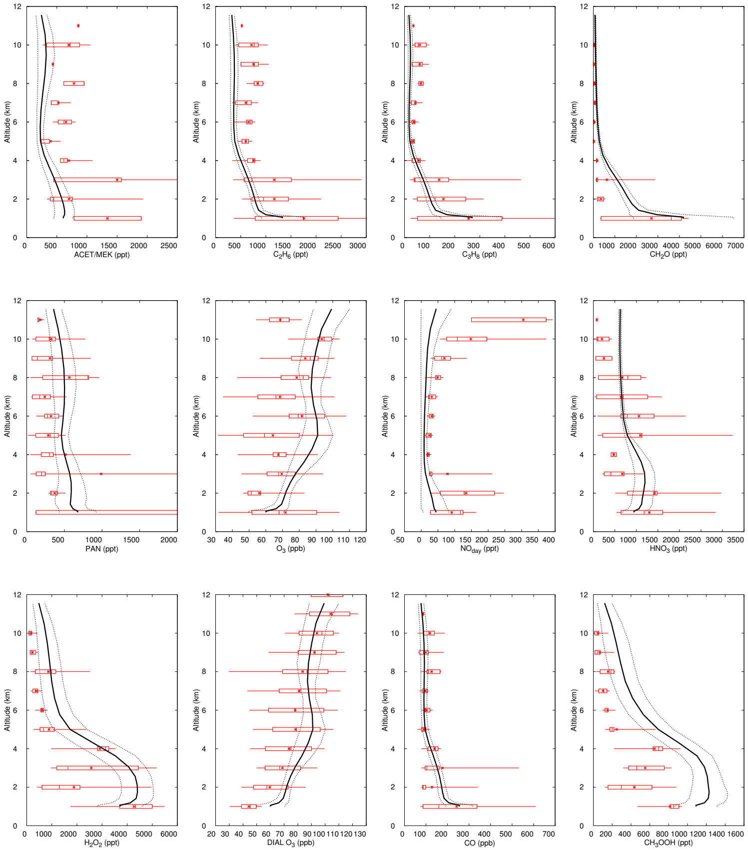

Fig. 10. Seasonally averaged profiles from TRACE-A (21 Sept–26 Oct 1992) and GEM-AQ for the same period in 2001.

Title Page
Abstract
Introduction
Conclusions
References
Tables
Figures
◀◀
▶▶
◀
▶
Back
Close
Full Screen / Esc
Printer-friendly Version
Interactive Discussion

EGU